Supporting Information

Rapid and manual-shaking exfoliation of amidoximated cellulose nanofibrils for large-capacity filtration capture of uranium

*Weihua Zhang[a,b], Xiao Han[b,c], Jun You[d], Xiaofang Zhang[b,c], Danfeng Pei[b,c], Stefan Willför,[a] Mingjie Li[*b,c], Chunlin Xu[*,] and Chaoxu Li[*b,c]*

[a] Laboratory of Natural Materials Technology, Åbo Akademi University, Henrikinkatu 2, Turku FI-20500, Finland

[b]Group of Biomimetic Smart Materials, Qingdao Institute of Bioenergy and Bioprocess Technology, Chinese Academy of Sciences & Shandong Energy Institute, Songling Road 189, Qingdao 266101, P.R. China

[c]Center of Material and Optoelectronics Engineering, University of Chinese Academy of Sciences, 19A Yuquan Road, Beijing 100049, P. R. China

[d]Key Laboratory for the Green Preparation and Application of Functional Materials, Hubei Key laboratory of Polymer Materials, School of Materials Science and Engineering, Hubei University, Youyi Road 368, Wuhan 430062, China

*Corresponding authors: Chaoxu Li (Email: licx@qibebt.ac.cn); Chunlin Xu (Email: chunlin.xu@abo.fi); Mingjie Li (Email: limj@qibebt.ac.cn).

Table of contents in Supporting Information:

Supporting experimental section

Adsorption in non-spiked natural seawater. The uranium uptake capacity was also determined in natural seawater without the addition of additional uranium. The adsorbents (5 mg) were soaked into natural seawater (50 L, collected from Yellow Sea of China, Qingdao, Shandong Province) for 7, 14, 21, and 30 days, followed by digesting under microwave digestion for 1 h, filtrating and diluting with deionized water, respectively. The uranium concentration was determined by ICP-MS.

Supporting figures

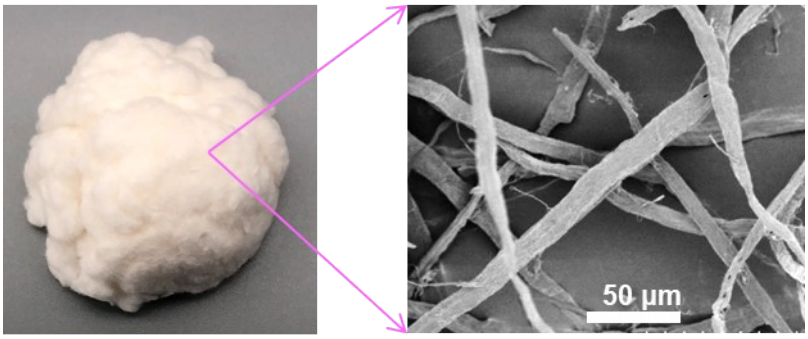

Fig. S1. Commercial softwood pulp.

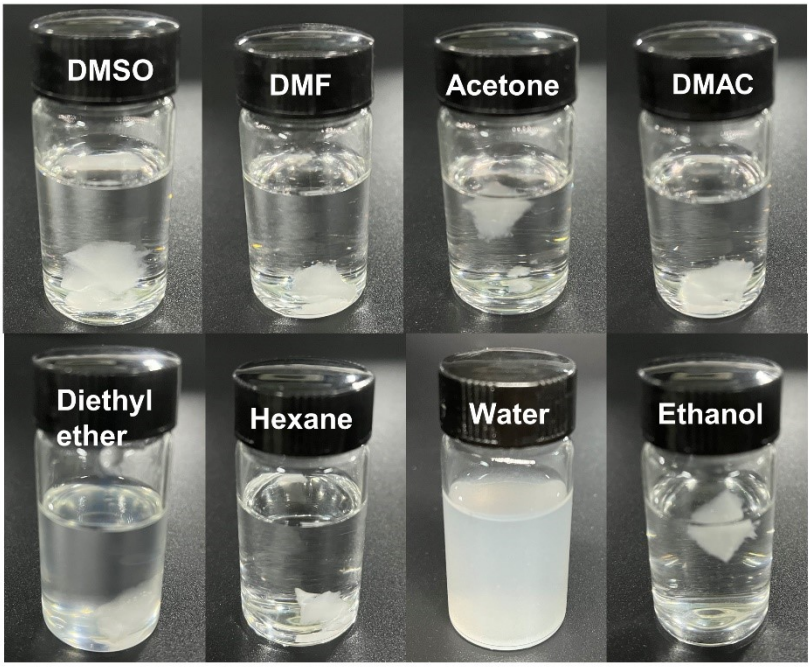

Fig. S2. Photographs of freeze-dried mechanically grinded cellulose nanofibers in various solvents.

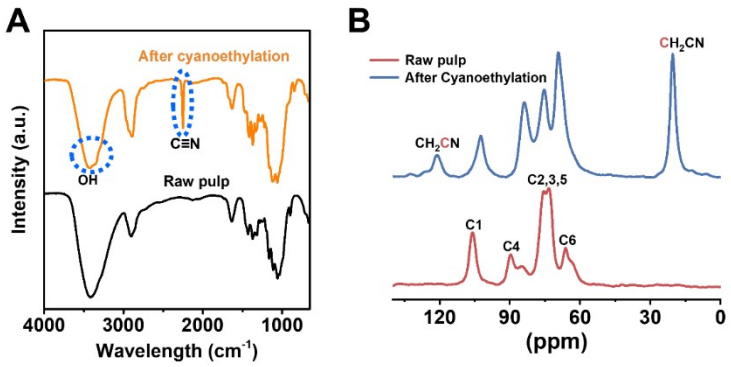

Fig. S3. FT-IR spectra (A) and solid-state 13C NMR spectra (B) of cellulose pulp before and after cyanoethylation.

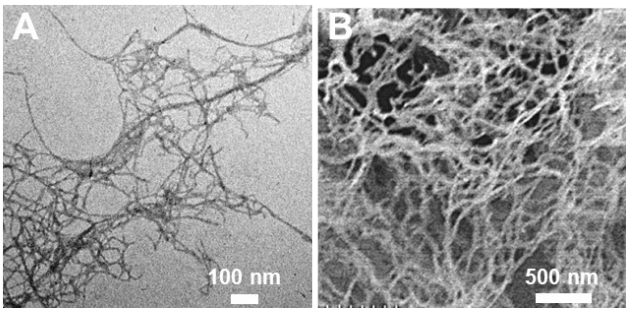

Fig. S4. TEM (A) and SEM (B) images of cyanoethylated cellulose nanofibrils. Cyanoethylated *DS:* ~1.58.

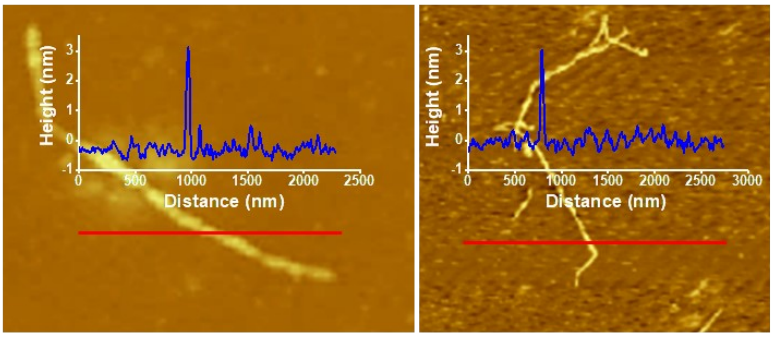

Fig. S5. AFM images of cyanoethylated cellulose nanofibrils. Cyanoethylated *DS:* ~1.58.

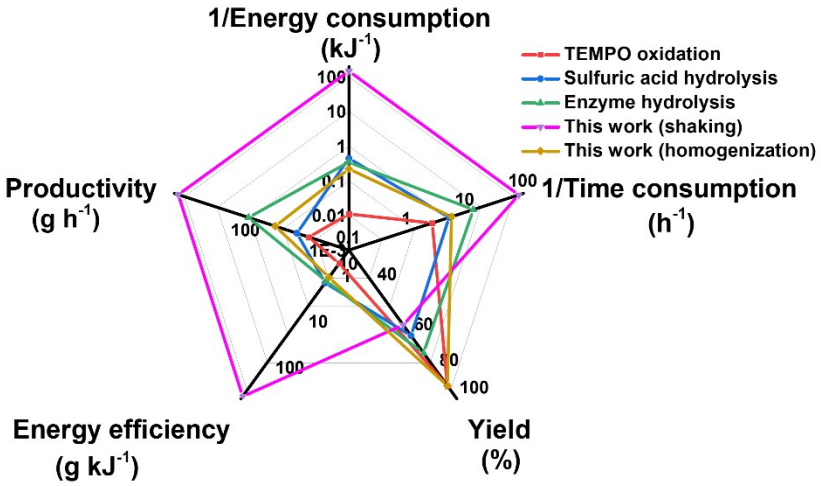

Fig. S6. Production characteristics of cyanoethylated cellulose fibrils in comparison to other production methods of cellulose fibrils.

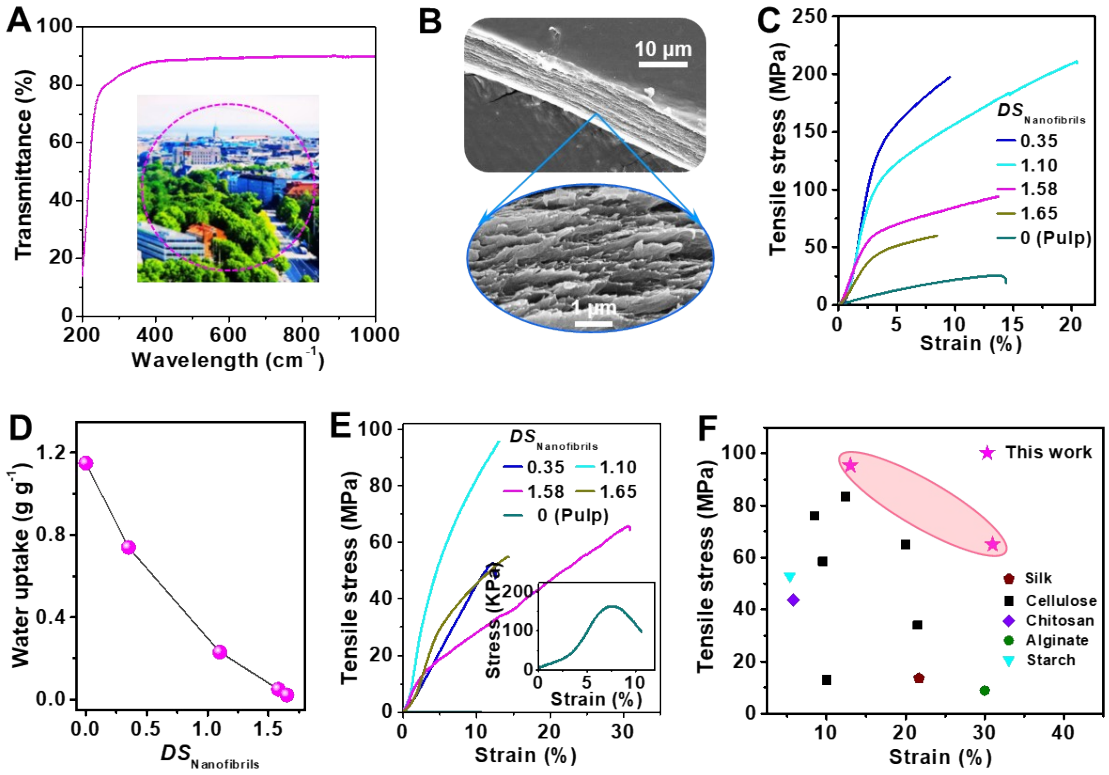

Fig. S7. Physical characterization of film of cyanoethylated cellulose fibrils. (A) Transparency evaluated by UV-vis transmittance. (B) Cross-sectional SEM images. (C) Stress-strain curves with indicated cyanoethylated *DS* values. (D) Influence of cyanoethylated *DS* values on water uptake. (E) Stress-strain curves at wet states with indicated cyanoethylated *DS* values. (F) mechanical performances at wet states in comparison to other biopolymers.

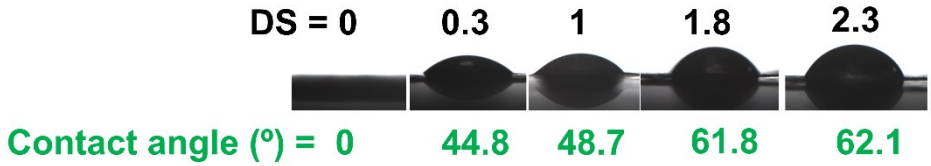

Fig. S8. Water contact angle measured on the cyanoethylated cellulose fibrils films with different *DS* values.

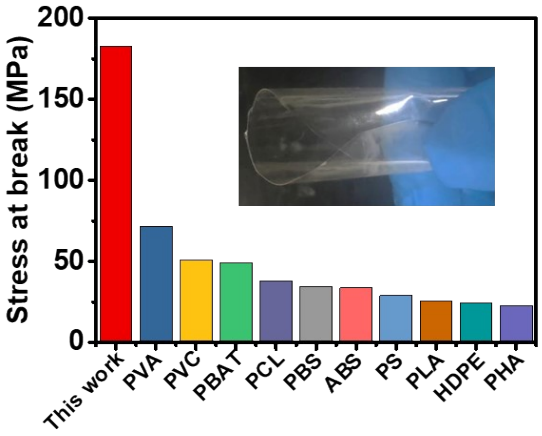

Fig. S9. Tensile stress at break of film of cyanoethylated cellulose fibrils in comparison to other synthetic polymers [1]. Polyvinyl alcohol: PVA; Poly vinyl chloride: PVC; Poly(butylene adipate-co-terephthalate): PBAT; Polycaprolactone: PCL; Polybutylene succinate: PBS; Acrylonitrile butadiene styrene: ABS; Polystyrene: PS; Polylactic acids: PLA; High-density polyethylene: HDPE; Polyhydroxyalkanoates: PHAs.

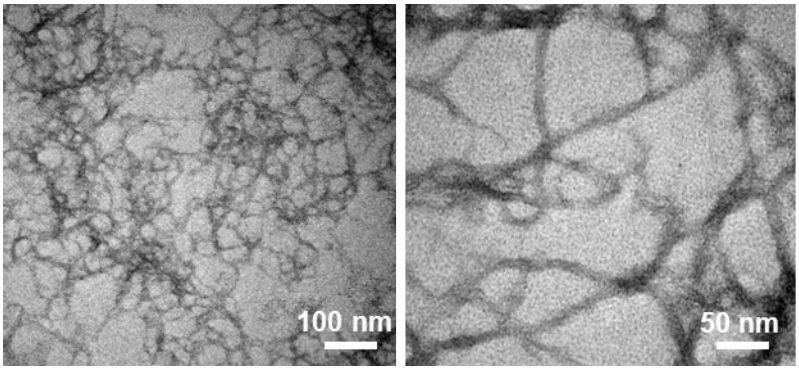

Fig. S10. TEM images of amidoximated cellulose nanofibrils. Amidoximated *DS*: ~1.58.

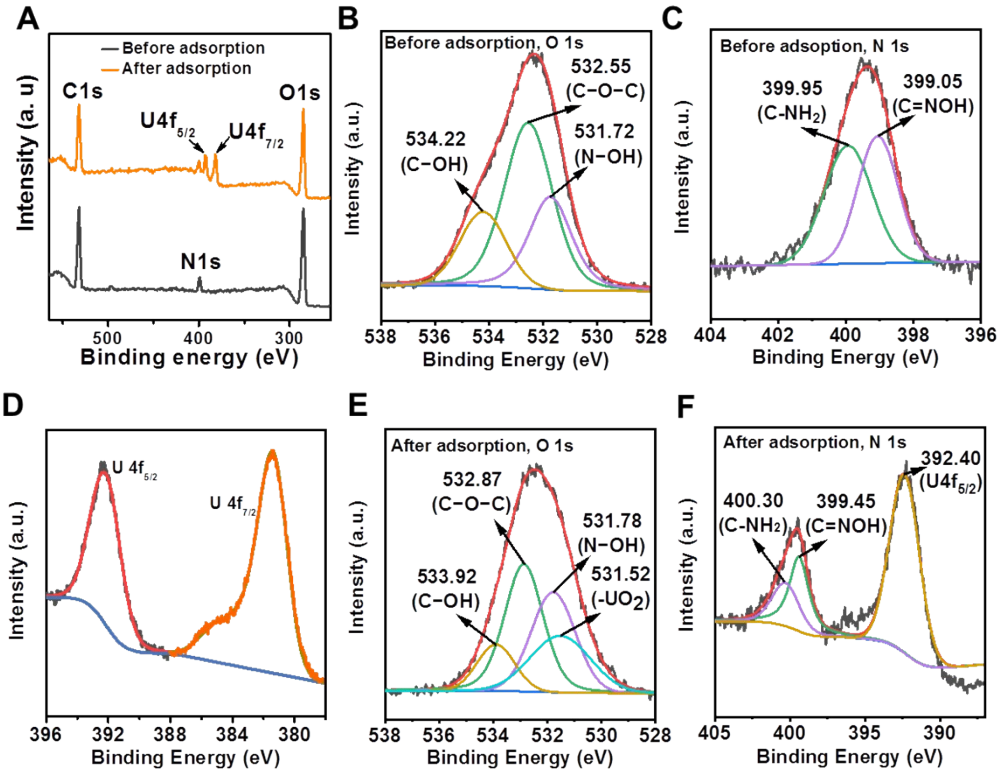

Fig. S11. (A,D) XPS spectra confirmed the uranium adsorption: (A) Wide-range XPS spectra of amidoximated cellulose nanofibrils before and after uranium adsorption; (D) High-resolution XPS spectra of U4f peaks of amidoximated cellulose nanofibrils after uranium adsorption. (B,E) XPS spectra and high-resolution spectra (O1s) of amidoximated cellulose nanofibrils before and after uranium adsorption. O1s profiles decomposed into three peaks at 534.22, 532.55 and 531.72 eV, which are assigned to the C−OH, C−O−C and N−OH. After uranium adsorption, the NOH peak shifted to 531.78 eV; and a new peak at 531.55 eV (assigned to the O=U=O) was detected, which confirmed the chelation between uranyl ions and amidoxime groups. (C,F) XPS spectra and high-resolution spectra (N1s) of amidoximated cellulose nanofibrils before and after uranium adsorption. Before uranium adsorption, the N1s peak of amidoximated cellulose nanofibrils deconvoluted in two peaks at 399.95 eV and 399.05 eV, assigned to the nitrogen of C-NH_2 and C=NOH groups[2, 3]. After uranium adsorption, three peaks were observed at 400.30 eV assigned for NH_2, at 399.45 eV for NOH and at 392.40 eV for $U4f_{5/2}$ due to complexation of U(VI) with oxime.

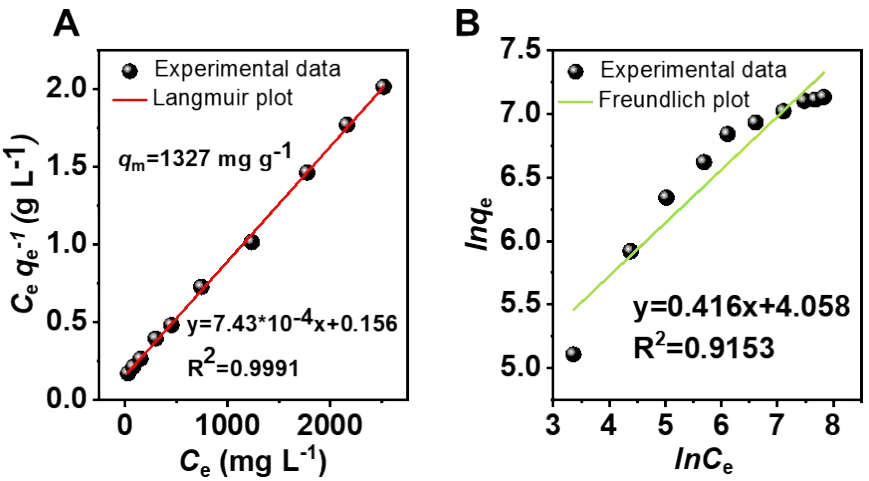

Fig. S12. Linearlized Langmuir (A) and Freundlich (B) isothermal models.

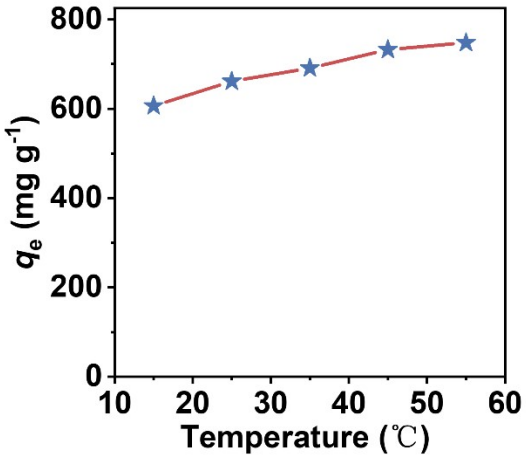

Fig. S13. Influence of temperature on the uranium adsorption performance. C_0 = 500 mg L^{-1}; pH 8.

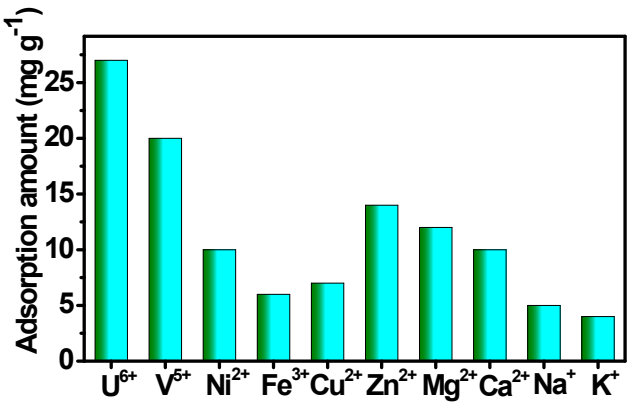

127

128 **Fig. S14.** Selectivity of amidoximated cellulose nanofibrils to indicated element ions in 100×

129 their natural concentration in simulated seawater for 24 h.

130

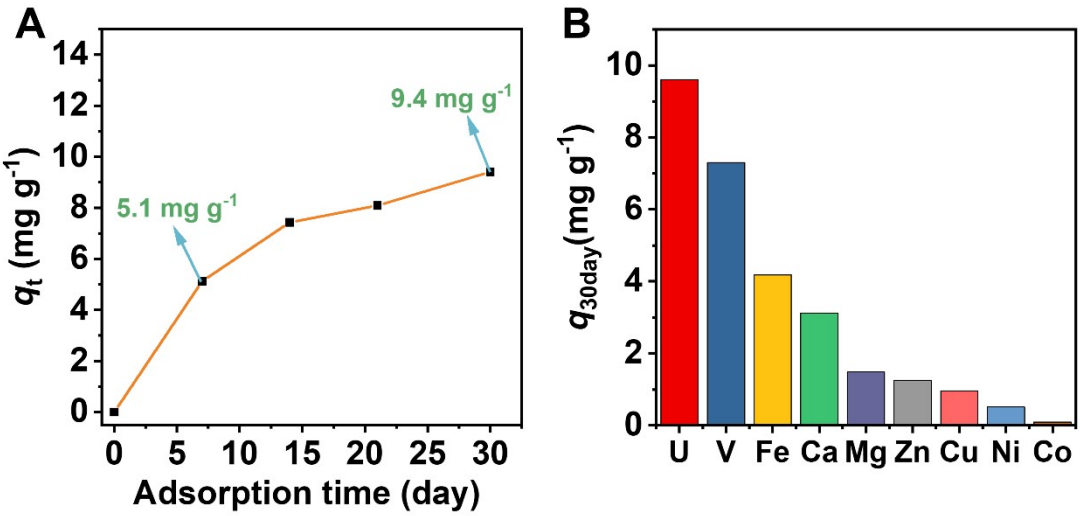

131

132 **Fig. S15.** (A) Uranium adsorption kinetics in natural seawater. (B) Capacities of uranium and

133 co-existing ions after adsorption in natural seawater for 30 days.

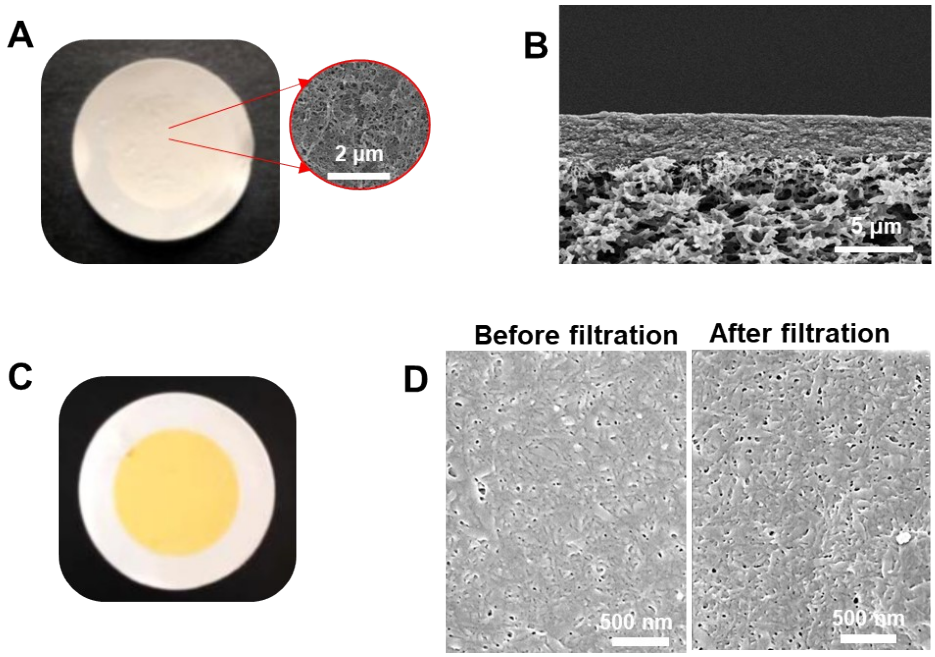

134

135 **Fig. S16. (**A) Photograph and SEM image of surface morphology of amidoximated cellulose
136 nanofibril film. (B) Cross-sectional SEM image of amidoximated cellulose nanofibril film. (C)
137 Photograph of amidoximated cellulose nanofibril film after uranium filtration. (D) SEM
138 images of surface morphology of amidoximated cellulose nanofibril film before and after
139 uranium filtration.

140

Supporting tables

Table S1. Calculation of total energy-consumption and time-consumption for different nanocellulose preparation.

Treatment of 1 kg raw cellulose pulp	Total time consumption (h)	Yield (%)	Total energy consumption (KJ)	Energy consumption (KJ g_{Fibril}^{-1})	Production speed (g_{Fibril} h^{-1})	Ref.
TEMPO Oxidation (Homogenization)	36.7	90	91152	101.3	24.5	[4]
TEMPO Oxidation (sonification)	186.7	70	181152	258.8	3.7	[4]
Sulfuric acid hydrolysis	18.7	60	22435	37.4	32.0	[5]
Enzyme hydrolysis	7.3	69	28876	41.8	94.5	[6]
Cyanoethylation-induced xfoliation (Homogenization)	17.3	90	45034	31.7	82	This work
Cyanoethylation-induced xfoliation (shaking)	1.2	58	69	0.08	700	This work

Table S2. Degree of substitution (*DS*) of cellulose pulp after different cyanoethylated reaction time. C, N and H element content were evaluated by Elemental analysis.

Reaction time (min)	C content (wt%)	N content (wt%)	H content (wt%)	DS
0	41.95	0	6.16	0
5	44.09	2.30	6.76	0.29
15	48.03	6.43	6.32	0.98
30	52.82	9.93	6.01	1.81
60	53.69	11.27	6.01	2.26
120	54.37	11.80	6.02	2.47

Table S3. Parameters of adsorption isotherm of amidoximated cellulose nanofibrils for U(VI) adsorption.

Sample	Langmuir			Freundlich		
	b	q_m	R^2	k_f	n_f	R^2
amidoximated cellulose nanofibrils	0.006	1327	0.9981	188.93	4.03	0.9261

Table S4. Comparison of amidoximated cellulose nanofibrils for U(VI) adsorption with various adsorbents.

Adsorbents	Time (min)	Adsorption capacity in simulated water (mg g^{-1})	Adsorption capacity in natural seawater (mg g^{-1})	pH	Reference
SiO_2-AO[a]	10	955.8	/	8	7
UiO-66[b]	720	346.89	4.62	6	8
AO-COF[c]	30	408	/	6	9
AO-HNTs[d]	1200	453.6	9.01	7	10
$[NH_4]^+[COF\text{-}SO_3^-]$[e]	210	851	/	5	11
DSHM-DAMN[f]	75	601	/	8	12
AO-Fe_3O_4@SiO_2[g]	240	105	/	5	13
NDA-TN-AO[h]	900	589.1	6.07	5	14
COF-PDAN-AO[i]	25	410	-	4	15
COF-HHTF-AO[j]	30	550.1	5.12	7	16
BD-TN-AO[k]	900	562	5.68	5	17
Bd-DBD[l]	300	1006.5	7.29	6	18
POP-PO_3H_2[m]	20	501	5.01	5	19
In-situ polymerized LDH[n]	400	1456	/	7	20
MF-HTC[o]	60	2208	/	3	21
PHO-CNF[p]	60	1550	/	6	22
SMON–PAO[q]	1800	1650	9.59	8	23
Amidoximated cellulose nanofibrils	3.5	1327	9.4	8	This work
Silk-nanofibrils	5	14.5	/	8	This work
Chitin-nanofibrils	6	25.6	/	8	This work
Tempo-cellulose nanofibrils	3	181.6	/	8	This work
Lysozyme-nanofibrils	8	30.1	/	8	This work

[a]Amidoxime functionalized silica framework (SiO_2-AO); [b]Antibacterial UiO-66 metal-organic frameworks (Anti-UiO-66); [c]Amidoxime-functionalized covalent organic frameworks (AO-COF); [d]Amidoxime-functionalized halloysite nanotubes adsorbents (AO-HNTs); [e]Ammoniating SO_3H-decorated covalent organic framework ($[NH_4]^+[COF\text{-}SO_3^-]$); [f]Diaminomaleonitrile (DAMN) functionalized double-shelled hollow (DSHM) metal-organic framework (DSHM-DAMN); [g]Amidoxime modified Fe_3O_4@SiO_2 (AO-Fe_3O_4@SiO_2);

[h]Naphthalene-based sp2-carbon amidoxime-functionalized covalent organic frameworks (NDA-TN-AO); [i]Carbon-conjugated amidoxime-functionalized covalent organic frameworks (COF-PDAN-AO); [j]Amidoxime functionalized two-dimensional (2D) polyarylether-based covalent organic frameworks (COF-HHTF-AO); [k]Amidoxime crystalline covalent organic framework (BD-TN-AO); [l]Benzoxazole-based covalent organic frameworks(Bd-DBD); [m]Porous organic polymer-PO_3H_2 (POP-PO_3H_2); [n]Polymer intercalated hybrid layered double hydroxide (LDH); [o]Magnesium ferrite loaded hydrothermal carbon (MF-HTC); [p]Phosphorylated cellulose nanofibers (PHO-CNF); [q]Porous amidoxime-based nanofiber adsorbent (SMON-PAO).

Supporting references

1. Q. Xia, C. Chen, Y. Yao, J. Li, S. He, Y. Zhou, T. Li, X. Pan, Y. Yao and L. Hu, *Nat. Sustain.*, 2021, **4**, 627-635.
2. J. Wu, K. Tian and J. Wang, *Prog. Nucl. Energ.*, 2018, **106**, 79-86.
3. X. L. Wang, Y. Li, J. Huang, Y. Z. Zhou, B. L. Li and D. B. Liu, *J. Environ. Radioactiv.*, 2019, **197**, 81-89.
4. Q. Li, S. Mcginnis, C. Sydnor, A. Wong and S. Renneckar, *ACS Sustain. Chem. Eng.*, 2013, **1**, 919-928.
5. S. Beck-Candanedo, M. Roman and D. G. Gray, *Biomacromolecules*, 2005, **6**, 1048-1054.
6. M. Paako, M. Ankerfors, H. Kosonen, A. NykaNen, S. Ahola, M. Osterberg, J. Ruokolainen, J. Laine, P. T. Larsson and O. Ikkala, *Biomacromolecules*, 2007, **8**, 1934-1941.
7. M. Ahmad, J. Wang, Z. Yang, Q. Zhang and B. Zhang, *Chem. Eng. J.*, 2020, **389**, 124441.
8. Q. Yu, Y. Yuan, J. Wen, X. Zhao, S. Zhao, D. Wang, C. Li, X. Wang and N. Wang, *Adv. Sci.*, 2019, **6**, 1900002.
9. Q. Sun, B. Aguila, L. D. Earl, C. W. Abney, L. Wojtas, P. K. Thallapally and S. Ma, *Adv. Mater.*, 2018, **30**, 1705479.
10. S. Zhao, Y. Yuan, Q. Yu, B. Niu, J. Liao, Z. Guo and N. Wang, *Angew. Chem. Int. Edit.*, 2019, **131**, 15121-15127.
11. X. H. Xiong, Z. W. Yu, L. L. Gong, Y. Tao, Z. Gao, L. Wang, W. H. Yin, L. X. Yang and F. Luo, *Adv. Sci.*, 2019, **6**, 1900547.
12. J. Zhang, H. Zhang, Q. Liu, D. Song, R. Li, P. Liu and J. Wang, *Chem. Eng. J.*, 2019, **368**, 951-958.
13. Y. Zhao, J. Li, L. Zhao, S. Zhang, Y. Huang, X. Wu and X. Wang, *Chem. Eng. J.*, 2014, **235**, 275-283.
14. W. R. Cui, F. F. Li, R. H. Xu, C. R. Zhang, X. R. Chen, R. H. Yan, R. P. Liang and J. D. Qiu, *Angew. Chem. Int. Edit.*, 2020, **132**, 17837-17843.
15. F.-F. Li, W.-R. Cui, W. Jiang, C.-R. Zhang, R.-P. Liang and J.-D. Qiu, *J. Hazard. Mater.*, 2020, **392**, 122333.
16. G. Cheng, A. Zhang, Z. Zhao, Z. Chai, B. Hu, B. Han, Y. Ai and X. Wang, *Sci. Bull.*, 2021, **66**, 1994-2001.
17. C.-R. Zhang, W.-R. Cui, R.-H. Xu, X.-R. Chen, W. Jiang, Y.-D. Wu, R.-H. Yan, R.-P. Liang and J.-D. Qiu, *CCS Chem.*, 2021, **3**, 168-179.
18. W. R. Cui, C. R. Zhang, R. H. Xu, X. R. Chen, R. H. Yan, W. Jiang, R. P. Liang and J. D. Qiu, *Small*, 2021, **17**, 2006882.
19. Q. Sun, Y. Song, B. Aguila, A. S. Ivanov, V. S. Bryantsev and S. Ma, *Adv. Sci.*, 2021, **8**, 2001573.
20. A. Jana, A. Unni, S. S. Ravuru, A. Das, D. Das, S. Biswas, H. Sheshadri and S. De, *Chem. Eng. J.*, 2022, **428**, 131180.
21. X. Li, Y. Li, Q. Wu, M. Zhang, X. Guo, X. Li, L. Ma and S. Li, *Chem. Eng. J.*, 2019, **365**, 70-79.
22. J. Lehtonen, J. Hassinen, A. A. Kumar, L.-S. Johansson, R. Mäenpää, N. Pahimanolis,

T. Pradeep, O. Ikkala and O. J. Rojas, *Cellulose*, 2020, **27**, 10719-10732.
23. Y. Yuan, S. Zhao, J. Wen, D. Wang, X. Guo, L. Xu, X. Wang and N. Wang, *Adv. Funct. Mater.*, 2019, **29**, 1805380.